This is an *Accepted Manuscript*, which has been through the Royal Society of Chemistry peer review process and has been accepted for publication.

Accepted Manuscripts are published online shortly after acceptance, before technical editing, formatting and proof reading. Using this free service, authors can make their results available to the community, in citable form, before we publish the edited article. We will replace this *Accepted Manuscript* with the edited and formatted *Advance Article* as soon as it is available.

You can find more information about *Accepted Manuscripts* in the **Information for Authors**.

Please note that technical editing may introduce minor changes to the text and/or graphics, which may alter content. The journal's standard **Terms & Conditions** and the **Ethical guidelines** still apply. In no event shall the Royal Society of Chemistry be held responsible for any errors or omissions in this *Accepted Manuscript* or any consequences arising from the use of any information it contains.

ARTICLE TYPE

Structure-Property Relations of Novel Microwave Dielectric ceramics with Low Sintering Temperatures: $(Na_{0.5x}Bi_{0.5x}Ca_{1-x})MoO_4$

Jing Guo,[a] Di Zhou,[a] Yong Li,[a] Tao Shao,[b] Ze-Ming Qi,[b] Biao-Bing Jin,[c] and Hong Wang,[*a]

Novel series of microwave dielectric ceramics $(Na_{0.5x}Bi_{0.5x}Ca_{1-x})MoO_4$ ($0 \leq x \leq 0.6$) was synthesized by the solid state reaction method. The crystal structures, microstructures, dielectric responses, and vibrational properties were investigated using X-ray diffraction, scanning electron microscopy, microwave network analyzer, terahertz, Raman and infrared spectroscopies. All the samples can be sintered well below 850
10 °C and a scheelite solid solution can be formed without any secondary phase. At x = 0.5 and x = 0.6, low-firing (750~775 °C) high performance microwave dielectric materials were obtained with permittivities of 19.1~21.91, Q×f values of 20,660~22,700 GHz, and near-zero temperature coefficients. The factors affecting microwave dielectric properties were discussed based on the vibrational data. As revealed by the Raman spetroscopy, the disorder degree grows with x rising, which might increase the permittivities and
15 decrease the Q×f values. The infrared spectra were analyzed using the classical harmonic oscillator model, and the complex dielectric responses gained from the fits were extrapolated down to the microwave and THz range. It is believed that the external vibration modes located at low frequencies dominate the main dielectric polarization contributions, especially the Na-O/Bi-O translational mode. This result indicates that the microwave dielectric properties of $(Na_{0.5x}Bi_{0.5x}Ca_{1-x})MoO_4$ ceramics mainly depend on the
20 behavior of AO_8 polyhedrons.

Introduction

Since 1990s, the rapid development of wireless communication technology has led to extensive research of microwave dielectric materials, which can be used as dielectric resonators, filters,
25 substrates, and antennas. In order to meet the miniaturization and integration demands, low temperature co-fired ceramic (LTCC) technology appeared and has been widely studied. The required key properties for microwave dielectric materials are low sintering temperatures (lower than the melting point of the base
30 metal electrodes, silver-961 °C or copper-1042 °C), suitable permittivities, high quality factor (Q×f) values, and near zero temperature coefficients of resonant frequency (TCF/$\tau_f \approx 0$ ppm/°C). There is a need to search for new materials with potentials for the LTCC application. Furthermore, the
35 relationships between dielectric properties and structures are also needed to be investigated.[1-6]

It is well known that scheelite-type ABO_4 (A= alkali metal, Ca^{2+}, Sr^{2+}, Ba^{2+}, Bi^{3+}, Ln^{3+}, etc. B=Mo^{6+}, W^{6+}) compounds are important functional materials in the field of scintillation
40 detectors, phosphors, lasers, photo-catalysts, and lithium-ion batteries.[7-11] Recently, some scientists reported that ABO_4 (A=Ca, Sr, Ba, B=Mo, W) ceramics also exhibit good microwave dielectric properties.[12,13] Among them, $CaMoO_4$ has a very high Q×f value of 89,700 GHz and a low permittivity of 10.79.
45 However, the high firing temperature (1100 °C) and large negative TCF value (-57 ppm/°C) limit its application. From the

view of crystal chemistry, if an ion or several ions substitute for Ca^{2+} (or Mo^{6+}) to form a solid solution, the change of the bonds may tune the sintering temperature and dielectric property.
50 $CaMoO_4$ has a tetragonal unit cell with space-group symmetry $I4_1/a$.[14] The A-site cation is coordinated by 8 oxygen anions by relatively weak forces, and the B-site cation is surrounded by 4 oxygen anions forming a tightly bound BO_4 tetrahedron, as illustrated in Fig. 1. Alkali and bismuth ions are potential ions to
55 tune the dielectric properties of scheelite materials.[15-18] The previous work shows that $(Na_{0.5}Bi_{0.5})MoO_4$ has a scheelite structure with a low sintering temperature (690 °C) and a positive TCF value (+43 ppm/°C).[19] Therefore, using Na^+ and Bi^{3+} ions to replace Ca^{2+}, it is possible to achieve a new material system
60 $(Na_{0.5x}Bi_{0.5x}Ca_{1-x})MoO_4$ with intrinsic low sintering temperatures and near zero TCF values. Additionally, the distribution of Na^+ and Bi^{3+} ions over the A sites may bring interesting structural changes, which helps to explore the correlation between structures and properties.

65 The dielectric properties at microwave frequencies mostly depend on ionic polarization caused by lattice vibrations. Therefore, vibrational spectroscopies are useful techniques to study the basics of microwave dielectric materials.[20-22] It was reported that microscopic composition fluctuations and order-
70 disorder state exist in the A site of $(Na_{0.5}Bi_{0.5})MoO_4$ crystal.[23,24] It can be speculated that similar phenomena may happen in the $(Na_{0.5x}Bi_{0.5x}Ca_{1-x})MoO_4$ ($0<x<1$) system, which lead to changes of dielectric properties and vibrational spectra. Raman spectra can provide short range characters of materials, including order-

disorder transitions. It helps to probe the mechanisms of dielectric behaviors. Infrared spectroscopy is also a powerful tool to study the behaviors of polar phonon modes. Dielectric losses are divided to intrinsic and extrinsic parts. Intrinsic losses are the losses in ideal defect-free materials. They are dependent on the crystal structure, ac field frequency and temperature. Extrinsic losses are caused by imperfections in the lattice, such as impurities, pores, grain sizes and shapes, order-disorder etc. [25-27] At the infrared frequencies, intrinsic losses are expected to predominate over extrinsic ones, which may result from known relation that many extrinsic loss mechanisms are unable to follow high frequencies. Furthermore, the broad frequency range of infrared spectra makes it possible to distinguish extrinsic loss contributions from intrinsic ones. The intrinsic losses may be estimated from the fits of infrared reflection spectra by the classical dispersion theory.[22]
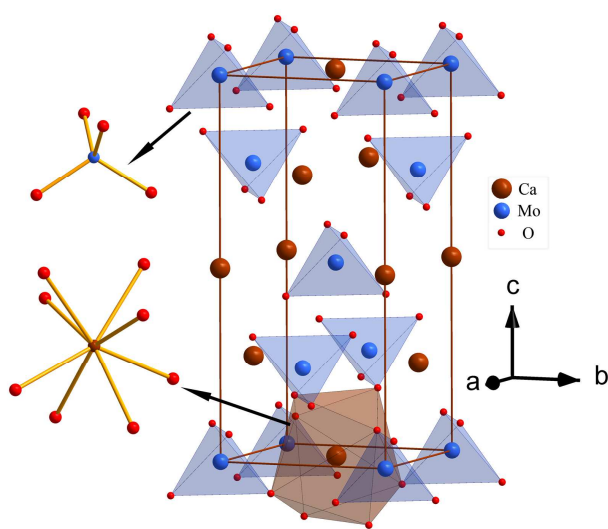

Fig. 1 Schematic illustrating the crystal structure of tetragonal $CaMoO_4$.

In the present work, new series of $(Na_{0.5x}Bi_{0.5x}Ca_{1-x})MoO_4$ ($0 \leq x \leq 0.6$) ceramics was prepared and their phase composition, sintering behavior, microstructure, and microwave dielectric properties were investigated. To achieve deeper understanding of the relations between structures and dielectric properties, Raman, infrared and terahertz spectroscopies were employed. The results were discussed based on the structure changes caused by the ion substitution at A sites.

Experimental

Polycrystalline samples of $(Na_{0.5x}Bi_{0.5x}Ca_{1-x})MoO_4$ (x=0, 0.1, 0.2, 0.4, 0.5, 0.6; NBCM were used for abbreviations) were synthesized by the mixed-oxide process. Reagent-grade powders Na_2CO_3 (>99.8%, Hongyan Chemical Reagents, Tianjin, China), Bi_2O_3 (>99%, Shudu Nano-Science Co., Ltd, Chengdu, China), $CaCO_3$ (>99%, Sinopharm Chemical Reagent Co. Ltd, Shanghai, China), and MoO_3 (>99.5%, Yutong Chemical Reagents, Tianjin, China) were used as starting materials. Stoichiometric amounts of powder mixtures were milled with ethanol and zirconia balls (2 mm in diameter) for 4 h using a planetary ball-mill. Then, the slurry was dried and calcined in air at 600-650 °C for 4 h. After re-milling with zirconia balls in ethanol for 4 h, the final powders were mixed with 5 wt. % polyvinyl alcohol (PVA) binder and then pressed into cylindrical pucks (10mm in diameter and 4-5mm in height) under a uniaxial pressure of 250 MPa. Finally, these samples were sintered at 700-900 °C for 2 h with a heating rate of 3 °C/min in the air.

The crystal structure and phase composition of sintered samples were investigated by X-ray diffraction with Cu Kα radiation (Rigaku D/MAX-2400 X-ray diffractometer, Tokyo, Japan). Before the XRD test, the sintered pellets were ground to fine powders with an agate mortar and pestle. The microstructures of sintered ceramics on the surfaces were observed using a scanning electron microscope (SEM, FEI, Quanta 250 F). The bulk densities of the sintered specimens were determined by the Archimedes' method. The dielectric properties at microwave frequencies were measured with a network analyzer (8720ES, Agilent, Palo Alto, CA) according to the $TE_{01\delta}$ shielded cavity method. The temperature coefficient of the resonant frequency was measured using a network analyzer and a temperature chamber (Delta 9023, Delta Design, Poway, CA) in the 25-85 °C region, and was calculated by the following equation:

$$TCF = \frac{f_{85} - f_{25}}{f_{25}(85-25)} \times 10^6 (ppm/℃)$$

(1)

where f_{25} and f_{85} were the resonant frequencies at 25 °C and 85 °C, respectively. The dielectric behaviors at terahertz frequencies from 0.2 to 1.2 THz (6.7-40 cm^{-1}) were obtained with a terahertz time-domain (THz TDS) spectroscopy (ADVAVTEST TAS7500SP, Tokyo, Japan). A passive mode-lock fiber laser with extremely short pulse width (<50 fs), low jitter (<50fs) and high power (>200 mW) is used to pump and gate respectively two GaAs photoconductive antennas for the generation and detection of THz wave.

The Raman spectra of polished samples were collected at room temperature with a Raman spectrometer (HR800, HORIBA Jobin Yvon). The Ar ion laser (514 nm) was used as an excitation source with an effective power of 20 mW. The infrared reflectivity spectra were obtained on polished samples with a Fourier-transform infrared (FTIR) spectrometer (IFS 66v/S Vacuum, Bruker Optik Gmbh, Germany) in the infrared beamline station (U4) at the National Synchrotron Radiation Lab (NSRL). A Ge-coated KBr beamsplitter and a high sensitivity DTGS detector were used for the mid-infrared measurement (500-4500 cm^{-1}), while a Mylar beamsplitter, and a high sensitivity DTGS detector were used in the far-infrared range (50-700 cm^{-1}). The infrared data were collected under vacuum (<5 mbar) environment and the wavenumber resolution was better than 2 cm^{-1}.

Results and discussion

Structure and Microstructure

Figure 2 presents the XRD patterns of $(Na_{0.5x}Bi_{0.5x}Ca_{1-x})MoO_4$ ($0.1 \leq x \leq 0.6$) ceramics sintered at optimal temperatures. No obvious secondary phase can be detected and all the diffraction peaks can be indexed as a tetragonal scheelite phase (PDF# 85-

0585). Therefore, a complete scheelite solid solution was obtained in the whole composition range. When the x value goes up from 0 to 0.6, the intensity of (101) peak decreases gradually which may be attributed to the cation disordering in the A sites

5 after substitution of Na^+ and Bi^{3+} for the Ca^{2+} ions.[28] It is also seen that, as x value increases, the peaks systematically shift to lower 2θ angle direction, which reveals an increase in the unit cell volume.
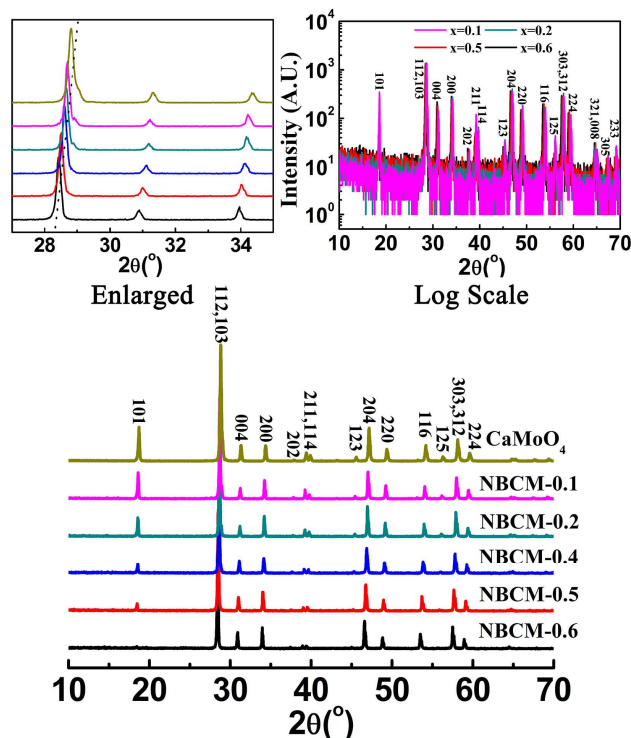

Fig. 2 X-ray diffraction patterns of the sintered $(Na_{0.5x}Bi_{0.5x}Ca_{1-x})MoO_4$ solid solutions.

According to the Shannon's data, the ionic radius of Na^{1+} (1.18Å) and Bi^{3+} (1.17Å) at 8 coordinated site is larger than that of Ca^{2+} (1.12Å) and the equivalent radius of A site

15 (r_A=1.12+0.055x Å) increases with the x value.[29] Consistent with the peak shift in the XRD patterns, the lattice constants (a, c) as well as the unit cell volume (V) of NBCM ceramics monotonically rise, as shown in Figure 3. Based on the tetragonal Scheelite structure (Figure 1), there are more A-site cations along

20 c axis than ones along a axis in the unit cell. The radius changes of A-site cations have a greater impact on the parameter c than parameter a. Consequently, the value of a/c declines as presented in Figure 3.

Figure 4 shows the SEM images of as-fired surfaces of

25 $(Na_{0.5x}Bi_{0.5x}Ca_{1-x})MoO_4$ (0.1≤x≤0.6) ceramics sintered at various temperatures (750-850 °C). Homogeneous microstructures can be seen. All the ceramics have well-packed grains and low porosity. For $(Na_{0.5x}Bi_{0.5x}Ca_{1-x})MoO_4$ (x=0.1, 0.2, 0.4, 0.5) samples, the grain sizes lie in the range of 3 ~ 9 μm, and the grain size of

30 $(Na_{0.5x}Bi_{0.5x}Ca_{1-x})MoO_4$ (x=0.6) sample is a little smaller (2 ~ 5 μm). From the backscattered electron image and EDS (energy dispersive spectrometer) analysis, it is seen that only one type grain exists, which is in accordance with the XRD analysis.
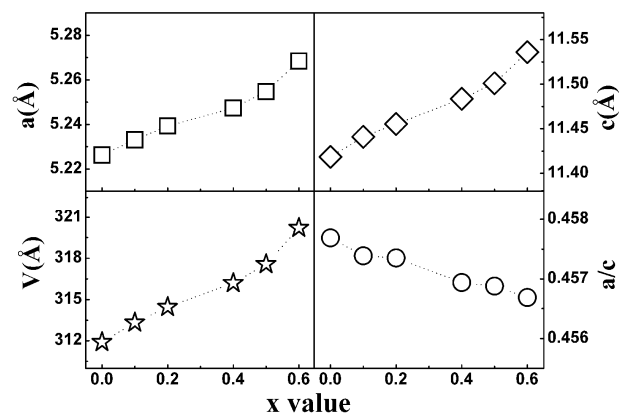
Fig. 3 Cell parameters of $(Na_{0.5x}Bi_{0.5x}Ca_{1-x})MoO_4$ ceramics as a function of the x value.
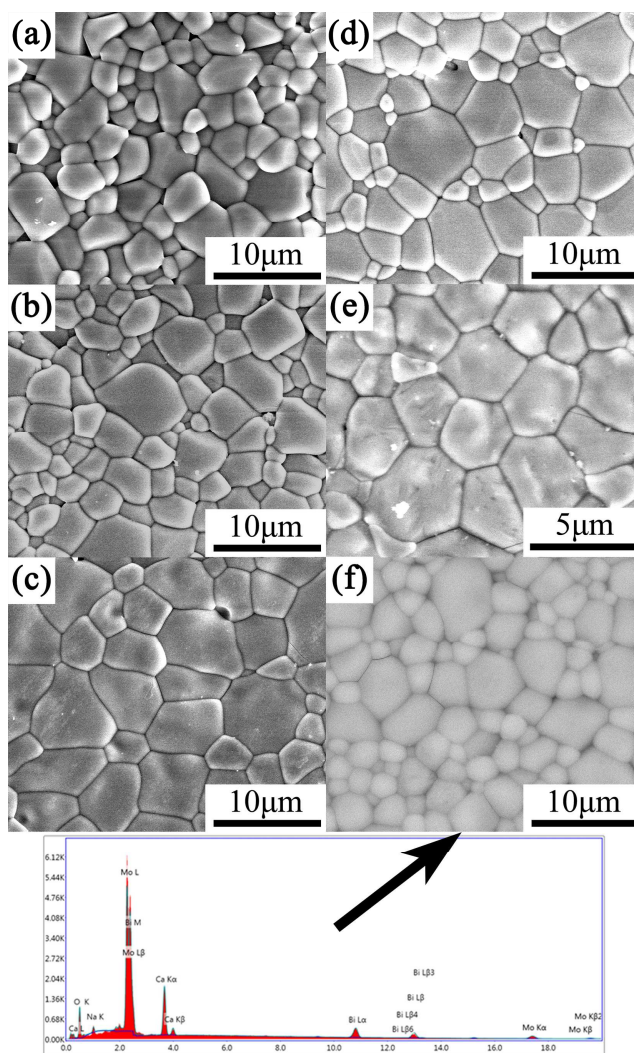
Fig. 4 SEM photos for NBCM-0.1 ceramic sintered at 850 °C for 2 h (a),
NBCM-0.2 ceramic sintered at 850 °C for 2 h (b), NBCM-0.4 ceramic
40 sintered at 800 °C for 2 h (c), NBCM-0.5 ceramic sintered at 775 °C for 2 h (d), and NBCM-0.6 ceramic sintered at 750 °C for 2 h (e), and the backscattered electron image of NBCM-0.5 ceramic sintered at 750 °C for 2 h (f).

Microwave Dielectric Properties

The densities and microwave dielectric properties of $(Na_{0.5x}Bi_{0.5x}Ca_{1-x})MoO_4$ ceramics are listed in Table.1. The densities go up from 4.215 g/cm^3 to 5.080 g/cm^3, with x in the 0.1-0.6 range. The relative densities of all specimens are over 95 %, suggesting that all the ceramics are well densified. The sintering temerature of NBCM ceramics as a function of x value is shown in Figure 5(a). Na_2O and Bi_2O_3 are low melting point oxides. Therefore, after Na^+ and Bi^+ ions replacing Ca^{2+} ions, the sintering temperature decreases and glass free low temperature fired microwave dielectric materials can be obtained.

The curve of permittivity versus x value is shown in Figure 5(b). When x value rises, there is a continuous increase in the measured permittivity of NBCM ceramics. The dielectric constants are also calculated by Clausius-Mosotti equation, as follows.

$$\varepsilon = \frac{3V_m + 8\pi\alpha_D}{3V_m - 4\pi\alpha_D} \quad (2)$$

where V_m and α_D is the molar volume and molecular

Table 1 Density and microwave dielectric properties of $(Na_{0.5x}Bi_{0.5x}Ca_{1-x})MoO_4$ ceramics

Sample	Sintering Temperature (°C)	Density (g/cm³)	Permittivity	Q×f (GHz)	TCF (ppm/°C)	Ref
$CaMoO_4$	1100	-	10.79	89,700	-57	12
$(Na_{0.5}Bi_{0.5})_{0.1}Ca_{0.9}MoO_4$	850	4.215	11.5	35,050	-51.6	This work
$(Na_{0.5}Bi_{0.5})_{0.2}Ca_{0.8}MoO_4$	850	4.392	13.3	32,860	-41.5	This work
$(Na_{0.5}Bi_{0.5})_{0.4}Ca_{0.6}MoO_4$	800	4.646	16.8	31,830	-17.3	This work
$(Na_{0.5}Bi_{0.5})_{0.5}Ca_{0.5}MoO_4$	775	4.916	19.1	22,700	-10.1	This work
$(Na_{0.5}Bi_{0.5})_{0.6}Ca_{0.4}MoO_4$	750	5.080	21.9	20,660	8.4	This work
$(Na_{0.5}Bi_{0.5})MoO_4$	690	-	34.4	12,300	+43	19

polarizability, respectively. The molecular polarizability of $(Na_{0.5x}Bi_{0.5x}Ca_{1-x})MoO_4$ can be derived using the ion additivity rule:[30]

$$\alpha_D (NBCM)=0.5x[\alpha_D (Na^{1+})+\alpha_D (Bi^{3+})]+(1-x)\alpha_D (Ca^{2+})+\alpha_D (Mo^{6+})+4\alpha_D (O^{2-}) \quad (3)$$

The ion polarizabilities of Na^{1+} (1.80), Bi^{3+} (6.12), Ca^{2+} (3.16), O^{2-} (2.01) and Mo^{6+} (3.28) are suggested by Shannon[30] and Choi.[12] With Na^{1+} and Bi^{3+} substitution, both the molecular polarizability and V_m increase, and the calculated permittivities have very small changes, as illustrated in Figure 5(b). It is seen that the measured permittivities are different from the calculated ones, and the deviations become larger and larger with x increasing. Shannon reported that the deviations may be attributed to piezo- or ferroelectric behavior, ionic or electronic conductivity, the presence of H_2O or CO_2 in channels, "rattling" or "compressed" cations, or dipolar impurities. Generally, "rattling" cations (smaller size) or "compressed" cations (larger size) have unusually large or small polarizabilities, respectively. However, these reasons cannot explain why the permittivities of NBCM ceramics increase with x value. The ionic radii of Na^{1+} and Bi^{3+} are larger than that of Ca^{2+}. According to the "compressed" cation theory, the permittivities should go down when Na^{1+} and Bi^{3+} substitute for Ca^{2+}. In fact, the permittivities go up in this study, which may be caused by "structural changes". The local atomic motion, disorder and polyhedral distortion are probably responsible for these large deviations. (The disorder characteristic will be discussed in the Raman spectra part) With Na^{1+} and Bi^{3+} substitution, the AO_8 dodecahedrons may adjust the configuration to adapt for the large cations. Because Na^{1+} and Bi^{3+} have different ionic radii, the disordered arrangement of Na and Bi ions at A site may also result in polyhedra distortions. Bond valence is a useful way to indicate the misfit of a cation at its site and may help to explain the deviations. The bond valences (V_i) of $CaMoO_4$ and $(NaBi)_{0.5}MoO_4$ were predicted by the most commonly used empirical expression:[31]

$$V_i = \Sigma_j \upsilon_{ij} \quad (4)$$

$$\upsilon_{ij} = exp[(R_{ij} - d_{ij})/b] \quad (5)$$

where υ_{ij} is a bond valence between two atoms i and j, R_{ij} is the bond valence parameter, d_{ij} is the length of a bond, and b is usually taken to be a universal constant. The bond valence parameters (R_{CaO}=1.967 Å, R_{NaO}=1.8 Å, R_{BiO}=2.09 Å, R_{MoO}=1.907 Å,) are on the basis of Brese's results. For $CaMoO_4$, the calculated bond valences of A-site, B-site and O-site are 2.082, 5.999, and 2.020, respectively. For $(NaBi)_{0.5}MoO_4$, the values of V_{A-site}, V_{B-site}, and V_{O-site} are 1.963, 5.696, and 1.915, respectively. It may be inferred that the bond strength becomes weaker when Na^+ and Bi^{3+} replace Ca^{2+}. This phenomenon reveals that, the misfit rate increases with the ion substitution amount in A site, which may make larger ion polarizabilities and thus increase the permittivities of NBCM ceramics.

Figure 5(c) plots the Q×f values of NBCM ceramics as a function of x value. It is seen that the Q×f values are sensitive to the A site substitution. With Na^{1+} and Bi^{3+} incorporation, the Q×f value deteriorates rapidly. However, when x varies from 0.1 to 0.6, there are only small changes in the Q×f values of NBCM samples. Q×f values can be affected by intrinsic factors and extrinsic factors. The XRD, SEM and density analysis shows that $(Na_{0.5x}Bi_{0.5x}Ca_{1-x})MoO_4$ (0.1 ≤ x ≤ 0.6) ceramics are complete scheelite solid solutions with high densities. The contributions of impurities and pores can be ignored. It is known that MoO_3, Na_2CO_3 and Bi_2O_3 may volatilize in the sintering process,[32-34] which may induce vacancies in the lattices. To some extent, these vacancies may affect the local structures of NBCM ceramics and decrease Q×f values. It could be expected that structure changes, including disordered charge distribution and polyhedral distortion, are main factors decreasing Q×f values. Figure 5(d) shows the TCF values of NBCM specimens. The TCF values of sintered NBCM ceramics shift from -57 to +8.4 ppm/°C with x value, and the near-zero TCF values are obtained at x=0.5 and x=0.6. Compared with the previous study on $BiVO_4$ doped with alkali and molybdenum ions,[15-18] NBCM ceramics with near-zero TCF values have smaller permittivities but higher Q×f values. However, they are all good candidates for microwave device
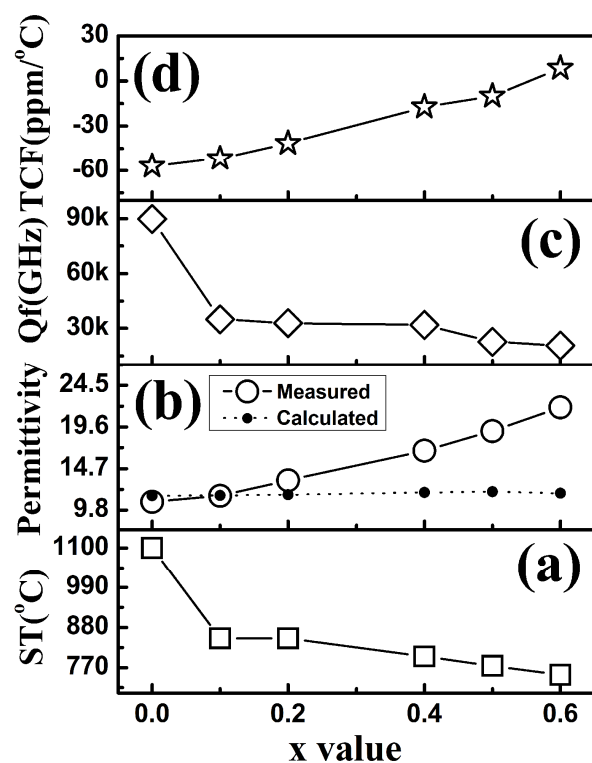
applications.

Fig. 5 Sintering temperatures, dielectric constants, Q×f values and TCF values of $(Na_{0.5x}Bi_{0.5x}Ca_{1-x})MoO_4$ ceramics as a function of x value.

Room Temperature Raman and Infrared Reflectivity Spectra

Based on the group theory analysis, there are 26 different vibrational modes for $CaMoO_4$ with the tetragonal structure, which are described as follows: [35]

$$\Gamma = 3A_g + 5B_g + 5E_g + 5A_u + 3B_u + 5E_u \qquad (6)$$

The even modes $3A_g$, $5B_g$ and $5E_g$ are Raman active, and the odd modes $4A_u$ and $4E_u$ are infrared active ($3B_u$ are inactive vibrations). According to the literature, the vibrations of $CaMoO_4$ can be subdivided into two groups: internal and external (lattice) modes. [35-38] The internal modes are related to the vibrations inside MoO_4 groups, whose centers of mass are considered stationary, and the external modes refer to the motions of Ca^{2+} cations and the rigid MoO_4 tetrahedron units, i.e., vibrations between lattice ions.

Figure 6 illustrates the room-temperature Raman spectra of $(Na_{0.5x}Bi_{0.5x}Ca_{1-x})MoO_4$ ($0.0 \leq x \leq 0.6$) ceramics in the range of 50 to 1000 cm^{-1}. There are 13 Raman active vibration modes in $CaMoO_4$. In this study, the A_g and B_g mode at 205-220 cm^{-1} and the $\nu_2(A_g)$ and $\nu_2(B_g)$ mode at 320-330 cm^{-1} is difficult to distinguish. Therefore, 11 Raman peaks are detected, among which the modes above 270 cm^{-1} are internal modes, and the peaks below 270 cm^{-1} belong to external modes. For the internal modes, ν_1 and ν_3 represents the stretching motions, and ν_2 and ν_4 stands for the bending motions. For the external modes, E_g (190 cm^{-1}) + A_g (205 cm^{-1}) are rotational modes, and the others are translational modes. All the Raman modes are in agreement with

the results reported in the literature. [35] When the x value rises, all the Raman bands become broader and many overlapping bands appear, as shown in Figure 6. These phenomena may result from the disorder arrangement of Na^+ and Bi^{3+} cations. In the perfect crystal of $(Na_{0.5}Bi_{0.5})MoO_4$, Na^+ and Bi^{3+} ions should form Bi-Na-Bi-Na layers perpendicular to c axis ($MoO_4Na_4Bi_4$ molecular system). But in fact, they may also form Bi-Bi-Na-Na layers (MoO_4Na_8 and MoO_4Bi_8 molecular systems) perpendicular to c axis. [23] This structural change may make Mo^{6+} ions occupy two different sites and deform MoO_4 tetrahedra which are correlated with the internal modes. It may be inferred that the MoO_4 tetrahedra become distorted with x>0. Consequently, there are more broad and overlapping bands in the internal region. The external modes of $(Na_{0.5x}Bi_{0.5x}Ca_{1-x})MoO_4$ ($x \neq 0$) ceramics are connected with not only Ca^{2+} ions and $[MoO_4]$ units, but also Na^+ and Bi^{3+} ions. It is known that the existence of Na^+ and Bi^{3+} ions may generate translational modes (52 cm^{-1}, 86 cm^{-1}) and coupled translational-rotational modes (133 cm^{-1}, 191 cm^{-1}). [39] Combined with the discussion of the disorder structure at A site, the Raman spectra in the external region have more active modes and the bands are broadened as the x value increases.
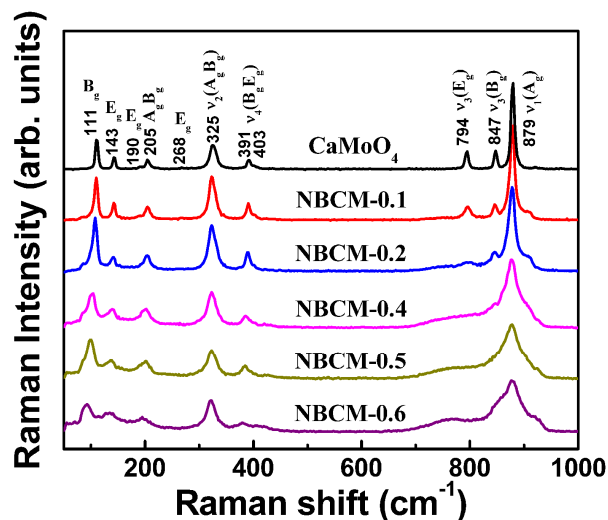

Fig. 6 Raman spectra for the $(Na_{0.5x}Bi_{0.5x}Ca_{1-x})MoO_4$ ceramics (ν_1, ν_2, ν_3, and ν_4: Internal modes; A_g, B_g, E_g: External modes)

Raman spectroscopy is powerful to characterize order-disorder phenomena. From the above analysis, it can be inferred that the degree of disorder increases with x going up. The disordering effects play an important role in behavior of dielectric properties. Ions with disordered distribution break the periodic arrangement of charges, so that the ionic polarizabilities may change and dielectric losses may increase. [40] Combined with the discussion on microwave dielectric properties of $(Na_{0.5x}Bi_{0.5x}Ca_{1-x})MoO_4$ ceramics, the growing disorder to some extent increases the samples' permittivities and decreases their Q×f values.

Figure 7 presents the IR reflectivity spectra of $(Na_{0.5x}Bi_{0.5x}Ca_{1-x})MoO_4$ ceramics ranging from 50 to 1200 cm^{-1}. It can be observed that all 8 IR active vibration modes of the $CaMoO_4$ ceramic are detectable, which consists with the vibrational analysis produced by other researchers. [35,41] There are 5 internal modes, located at 913 (ν_3-E_u), 897 (ν_3-A_u), 431 (ν_2-A_u), 329 (ν_4-E_u), and 284 (ν_4-A_u) cm^{-1}. Meanwhile, the peaks at 208 (E_u), 196

(A$_u$), and 150 (E$_u$) cm^{-1} are external modes. When Na^{1+} and Bi^{3+} substitute for Ca^{2+}, the [MoO$_4$] tetrahedra become distorted which possibly affect the position and intensity of peaks of internal modes. There are great changes in the vibration modes related to
5 stretching motions (ν_1 and ν_3). The ν_1 vibration (900-910 cm^{-1}) is activated in the IR spectra. [23] The original ν_3 vibration peaks at 913 and 897 cm^{-1} become weak and the new ν_3 vibration peaks at 823-833 and 752-667 cm^{-1} come out. Compared with vibration modes connected with stretching motions, the ν_2 and ν_4 modes
10 (bending motions) only have slight shifts. Similar to the Raman spectroscopy results, new external modes are generated by Na$^+$ and Bi^{3+} ions with x in the range of 0.1-0.6. From Fig.7, it can be observed that one of the major changes of external modes is the appearance of the new peak at the lowest wavenumber, 58-71 cm$^-$
15 ^{1}. According to the reference, this peak corresponds to the translational mode of Na-O and Bi-O, and T$_1$(Na,Bi) is used for abbreviations.[39]
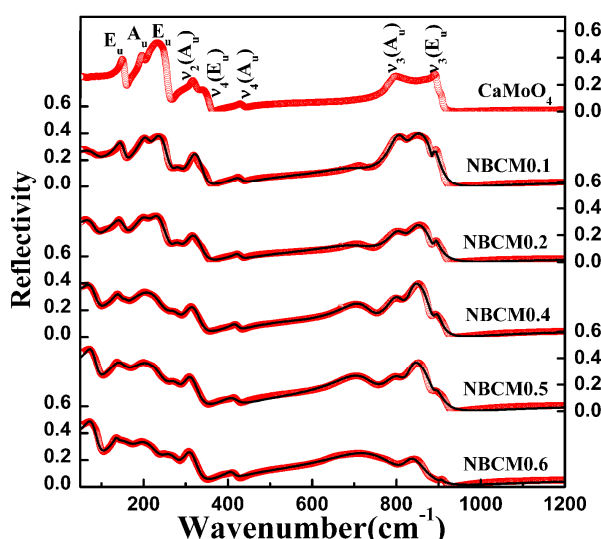

Fig. 7 Measured (red circles) and fitted (solid line) IR spectra for the
20 (Na$_{0.5x}$Bi$_{0.5x}$Ca$_{1-x}$)MoO$_4$ ceramics

These spectra have been analyzed by using the classical harmonic oscillator model based on the standard Lorentzian formula [Eqs7] and the Fresnel formula [Eqs8]:

$$\varepsilon^*(\omega) = \varepsilon_\infty + \sum_{j=1}^{n} \frac{\omega_{pj}^2}{\omega_{oj}^2 - \omega^2 - i\gamma_j\omega} \tag{7}$$

$$R(\omega) = \left| \frac{1 - \sqrt{\varepsilon^*(\omega)}}{1 + \sqrt{\varepsilon^*(\omega)}} \right|^2 \tag{8}$$

25 where $\varepsilon^*(\omega)$ is complex dielectric function; ε_∞ is the dielectric constant caused by the electronic polarization at high frequencies; ω_{pj}, ω_{oj} and γ_j are the plasma frequency, the transverse frequency (eigenfrequency), and damping factor of the j-th Lorentz
30 oscillator, respectively; n is the number of transverse phonon modes; R(ω) is the IR reflectivity. The spectra of NBCM

ceramics were fitted by 10-12 resonant modes which corresponded with the reflectivity peaks. The fitted spectra (solid line) are in good agreement with the experimental ones (circles),
35 as shown in Figure 7.

Figure 8 plots the calculated permittivity $\varepsilon'(\omega)$ and loss $\varepsilon''(\omega)$ obtained from the fits of the infrared reflectivity together with the experimental microwave and terahertz data. (One should note that these samples are partly absorbing in THz range.) It is seen that
40 the calculated permittivities are a little smaller than the measured ones in the microwave and THz ranges. Meanwhile, the calculated and measured dielectric losses have the same order of magnitudes. Therefore, it can be concluded that the microwave dielectric properties of NBCM ceramics are mainly caused by the
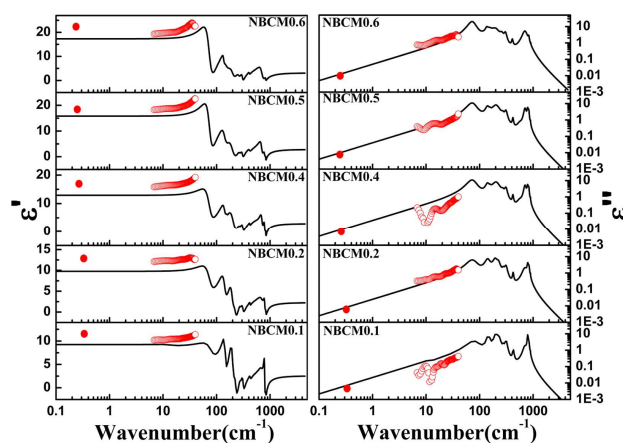45 polar optical phonons.[42]

Fig. 8 The real and imaginary parts of the complex dielectric response of (Na$_{0.5x}$Bi$_{0.5x}$Ca$_{1-x}$)MoO$_4$ ceramics. Red circles are experimental microwave
50 and terahertz data; Solid lines are the results from the fits of infrared spectra

Different vibration modes, associated with the crystal structure, may have different effects on the complex dielectric response. For scheelite-type ABO$_4$ materials, the BO$_4$ tetrahedron is tightly
55 bound while the AO$_8$ polyhedron is relatively loosened. They may behavior differently in the infrared range, so that it is meaningful to analyze the internal modes and external modes separatively. Under the condition of $\omega \ll \omega_{pj}$ (microwave frequency range), the ε' and tan(ω) can be derived from Eqs7,[40]

$$60 \quad \varepsilon' = \varepsilon_\infty + \sum_{j=1}^{n} \frac{\omega_{pj}^2}{\omega_{oj}^2} = \varepsilon_\infty + \sum_{j=1}^{n} \Delta\varepsilon_j \tag{9}$$

$$\tan\delta(\omega) = \frac{\varepsilon''}{\varepsilon'} = \omega \sum_{j=1}^{n} \frac{\Delta\varepsilon_j\gamma_j}{\omega_{oj}^2(\varepsilon_\infty + \sum_{j=1}^{n} \Delta\varepsilon_j)} \tag{10}$$

To keep consistent with the experimental data and to make it simple, the frequency ω is defined as 9 GHz. Figure 9 illustrates the influences of internal modes, external modes, and T$_1$(Na,Bi)
65 mode on dielectric properties. All the permittivities and losses are obtained from the above equations. It is seen that the internal

modes contribute only a small part of the permittivity and this contribution changes a little with x increasing. Nevertheless, the external modes take the most significant influences on the permittivity of NBCM ceramics. Among all the external modes, the T_1(Na,Bi) mode is the leading vibration mode whose contribution takes up almost 20-45% of the permittivities. Similarly, the dielectric losses related with external modes are 2 orders of magnitude larger than the losses caused by internal modes. The T_1(Na,Bi) mode is seen as the most important one in view of that its contribution to losses accounts for almost 70-85%. All these results indicate that, although MoO_4 tetrahedra become distorted and more internal modes come out with x rising, their contributions to permittivities and losses are small. For internal modes, after Na^+ and Bi^+ substituting for Ca^{2+}, more modes appear and they have remarkable effects on permittivities and losses. Especially, the T_1(Na,Bi) mode dominates the low frequency region of the infrared spectra and contributes the most part of dielectric properties. It can be inferred that the increasing microwave permittivities and decreasing Q×f values of NBCM ceramics are mainly attributed to the distortion of AO_8 polyhedrons.
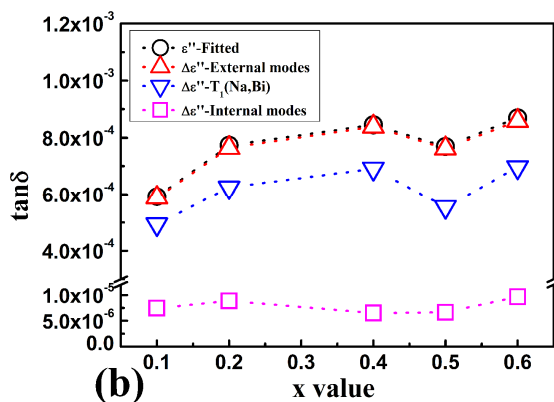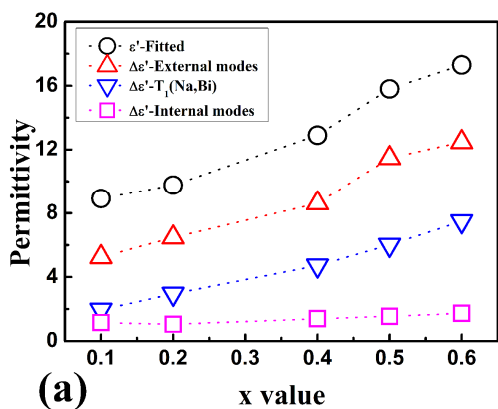

Fig. 9 The calculated dielectric properties of $(Na_{0.5x}Bi_{0.5x}Ca_{1-x})MoO_4$ ceramics as a function of x value

Conclusions

New glass-free low firing microwave dielectric materials $(Na_{0.5x}Bi_{0.5x}Ca_{1-x})MoO_4$ were investigated in this study. All the ceramics were well sintered below 850 °C. The XRD and SEM

pattern reveal that $(Na_{0.5x}Bi_{0.5x}Ca_{1-x})MoO_4$ (0.1≤x≤0.6) is a complete solid solution with tetragonal scheelite structure and no secondary phase can be detected over the composition range. As x varies from 0.1 to 0.6, the permittivities increase from 11.49 to 21.91, the Q×f values decrease from 35,050 to 20,660 GHz, and the TCF values shift from -51.6 to +8.4 ppm/°C. When x values were 0.5 and 0.6, temperature stable microwave dielectric materials with low sintering temperatures (ST=775~750 °C) were obtained with ε_r = 19.1~21.91, Q×f = 20,660~22,700 GHz, and |TCF| < 15 ppm/°C. The large deviations between the measured permittivities and the ones calculated by Clausius-Mosotti equation are probably attributed to the local atomic motion and disorder. The bond valence analysis indicates that the misfit rate rises with substitution in A site, which may lead to the distortion of AO_8 polyhedron and BO_4 tetrahedron. This misfit of cations may also change the ionic polarizabilities and helps to explain the deviations. In both Raman and infrared spectra, generation of new vibrational modes was caused by the structural change. The Raman spectra show that the degree of disorder grows with x, which may increase the samples' permittivities and decrease their Q×f values. The infrared spectra were fitted by 10-12 resonant modes corresponded with the infrared reflectivity peaks. The complex dielectric spectra gained from the fits were extrapolated down to the microwave and THz range. It could be seen that the external vibration modes contribute the most part of dielectric properties. Especially, the contribution of Na-O/Bi-O translational mode-T_1(Na,Bi) accounts for almost 20-45% of the permittivities and 70-85% of the losses. It may be inferred that the dielectric behaviors of $(Na_{0.5x}Bi_{0.5x}Ca_{1-x})MoO_4$ solid solutions mainly depend on the AO_8 polyhedron.

Notes and references

[a] Electronic Materials Research Laboratory, Key Laboratory of the Ministry of Education & International Center for Dielectric Research, Xi'an Jiaotong University, Xi'an, China, 710049. Fax: +86-29-82668794; Tel: +86-29-82668679; E-mail: hwang@mail.xjtu.edu.cn
[b] National Synchrotron Radiation Laboratory, University of Science and Technology of China, Hefei, Anhui, China, 230029
[c] Research Institute of Superconductor Electronics (RISE), School of Electronic Science and Engineering, Nanjing University, Nanjing, Jiangsu, 210093, China

1 W. Wersing, *Curr. Opin. Solid State Mat. Sci.*, 1996, **1**, 715-731.
2 R. J. Cava, *J. Mater. Chem.*, 2001, **11**, 54-62.
3 T. A. Vanderah, *Science*, 2002, **298**, 1182-1184.
4 I. M. Reaney and D. Iddles, *J. Am. Ceram. Soc.*, 2006, **89**, 2063-2072.
5 M. T. Sebastian and H. Jantunen, *Int. Mater. Rev.*, 2008, **53**, 57-90.
6 M. Valant and D. Suvorov, *J. Am. Ceram. Soc.*, 2000, **83**, 2721-2729.
7 V. B. Mikhailik, H. Kraus, G. Miller, M. S. Mykhaylyk and D. Wahl, *J. Appl. Phys.*, 2005, **97**, 083523.
8 N. Faure, C. Borel, M. Couchaud, G. Basset, R. Templier and C. Wyon, *Appl. Phys. B-Lasers Opt.*, 1996, **63**, 593-598.

9 L. S. Cavalcante, V. M. Longo, J. C. Sczancoski, M. A. P. Almeida, A. A. Batista, J. A. Varela, Mo. O. Orlandi, E. Longo and M. S. Liu, *CrystEngComm*, 2012, **14**, 853-868.

10 W. F. Yao and J. H. Ye, *J. Phys. Chem. B*, 2006, **110**, 11188-11195.

11 N. Sharma, K. M. Shaju, G. V. S. Rao, B. V. R. Chowdari, Z. L. Dong and T. J. White, *Chem. Mater.,* 2004, **16**, 504-512.

12 G. K. Choi, J. R. Kim, S. H. Yoon and K. S. Hong, *J. Eur. Ceram. Soc.,* 2007, **27**, 3063-3067.

13 S. H. Yoon, D. W. Kim, S. Y. Cho and K. S. Hong, *J. Eur. Ceram. Soc.,* 2006, **26,** 2051-2054.

14 E. Gurmen, E. Daniels and J. S. King, *J. Chem. Phys.,* 1971, **55**, 1093-1097.

15 D. Zhou, C. A. Randall, H. Wang, L. X. Pang and X. Yao, *J. Am. Ceram. Soc.*, 2010, **93**, 2147-2150.

16 D. Zhou, L. X. Pang, J. Guo, H. Wang, X. Yao and C. Randall, *Inorg. Chem.*, 2011, **50**, 12733-12738.

17 D. Zhou, W. G. Qu, C. A. Randall, L. X. Pang, H. Wang, X. G. Wu, J. Guo, G. Q. Zhang, L. Shui, Q. P. Wang, H. C. Liu and X. Yao, *Acta Mater.*, 2011, **59**, 1502-1509.

18 D. Zhou, L. X. Pang, H. Wang, J. Guo, X. Yao and C. A. Randall, *J. Mater. Chem.*, 2011, **21**, 18412-18420.

19 D. Zhou, C. A. Randall, L. X. Pang, H. Wang, J. Guo, G. Q. Zhang, Y. Wu, K. T. Guo, L. Shui and X. Yao, *Mater. Chem. Phys.*, 2011, **129**, 688-692.

20 A. Dias, L. A. Khalam, M. T. Sebstian, C. W. A. Paschoal and R. L. Moreira. *Chem. Mater.* 2006, **18**, 214-220.

21 J. Guo, D. Zhou, L. Wang, H. Wang, T. Shao, Z. M. Qi and X. Yao, *Dalton Transactions*, 2013, **42**, 1483-1491.

22 R. Zurmuhlen, J. Petzelt, S. Kamba, V.V. Voitsekhovskii, E. Colla, N. Setter, *J. Appl. Phys.* 1995, **77**, 5341-5350.

23 J. Hanuza, M. Maczka, L. Macalik and J. Vandermaas, *J. Mol. Struct.*, 1994, **325**, 119-124.

24 V. N. Moiseenko, Y. I. Bogatirjov, A. M. Jeryemenko and S. V. Akimov, *J. Raman Spectrosc.*, 2000, **31**, 539-541.

25 V. L. Gurevich and A. K. Tagantsev, *Adv. Phys.*, 1991, **40**, 719-767.

26 H. Tamura, *J. Eur. Ceram. Soc.*, 2006, **26**, 1775-1780.

27 S. J. Penn, N. M. Alford, A. Templeton, X. R. Wang, M. S. Xu, M. Reece and K. Schrapel, *J. Am. Ceram. Soc.*, 1997, **80**, 1885-1888.

28 D. Zhou, H. Wang, Q. P. Wang, X. G. Wu, J. Guo, G. Q. Zhang, L. Shui, X. Yao, C. A. Randall, L. X. Pang and H. C. Liu, *Funct. Mater. Lett.*, 2010, **3**, 253-257.

29 R. D. Shannon, *Acta Crystallogr. Sect. A*, 1976, **32**, 751-767.

30 R. D. Shannon, *J. Appl. Phys.*, 1993, **73**, 348-366.

31 N. E. Brese and M. Okeeffe, *Acta Crystallographica Section B-Structural Science*, 1991, **47**, 192-197.

32 Q. H. Zhang, Y. Y. Zhang, F. F. Wang, Y. J. Wang, D. Lin, X. Y. Zhao, H. S. Luo, W. W. Ge and D. Viehland, *Appl. Phys. Lett.*, 2009, **95**, 102904.

33 V. V. Atuchin, O. D. Chimitova, T. A. Gavrilova, M. S. Molokeev, S. J. Kim, N. V. Surovtsev and B. G. Bazarov, *J. Cryst. Growth*, 2011, **318**, 683-686.

34 V. V. Atuchin, V. G. Grossman, S. V. Adichtchev, N. V. Surovtsev, T. A. Gavrilova and B. G. Bazarov, *Opt. Mater.*, 2012, **34**, 812-816

35 S. P. S. Porto and J. F. Scott, *Phys. Rev.*, 1967, **157**, 716-719.

36 M. Nicol and J. F. Durana, *J. Chem. Phys.*, 1971, **54**, 1436-1440.

37 D. Christofilos, G. A. Kourouklis and S. Ves, *J. Phys. Chem. Solids*, 1995, **56**, 1125-1129.

38 T. T. Basiev, A. A. Sobol, Y. K. Voronko and P. G. Zverev, *Opt. Mater.*, 2000, **15**, 205-216.

39 J. Hanuza, A. Haznar, M. Maczka, A. Pietraszko, A. Lemiec, J. H. vanderMaas and E. T. G. Lutz, *J. Raman Spectrosc.*, 1997, **28**, 953-963.

40 K. Wakino, M. Murata and H. Tamura, *J. Am. Ceram. Soc.*, 1986, **69**, 34-37.

41 A. S. Barker, *Physical Review a-General Physics*, 1964, **135**, A742-A747.

42 J. Petzelt and S. Kamba, *Mater. Chem. Phys.*, 2003, **79**, 175-180.

Dalton Transactions Accepted Manuscript